Wideband CDMA Signal Propagation with Application to Smart Antennas

Noel T. Tin, *Member, IEEE*,
Steven D. Blostein†, *Senior Member, IEEE*

Abstract— **There is interest in increasing data rates of terrestrial wireless systems by increasing chip rates in code division multiple access (CDMA) systems, as well as by employing basestations equipped with smart antennas. We have constructed an experimental facility to assess certain key propagation effects in wideband CDMA (at 7 Mcps) employing digital multi-beamforming at a basestation receiver antenna array. One of the unique features of our system is that we employ multiple transmitters to experimentally assess the impact of multi-user interference. After characterizing the resolvable multipath, including the temporal dynamics, we study the spatial signatures received from four simultaneous users. We show that by processing the received data in blocks of 25 bits, it is possible to achieve a significant array gain (over 3 dB on average from 4 antennas) if the multi-user interference is taken into account via maximum signal-to-noise-plus-interference (SINR) beamforming. If the spatial signatures of users are too similar, however, these gains are not realized. Moreover, spatial signatures were not found to be predictable from users' physical locations.**

Keywords— **code division multiple access, smart antennas, multipath propagation**

I. Introduction

Experimental characterization studies of narrowband terrestrial mobile communication channels at $910MHz$ include [1] [2] [3]. Here, Doppler fading effects are predominant since relatively long data symbols are used. Higher data rates introduce significant dispersion due to multipath delay spread. More recent efforts concerning antenna arrays in the 1.8-2.0 GHz band [4] [5] [6] [7] [8] are directed toward direction of arrival (DOA) estimation, multipath characterization and beamforming performance assessment in mobile communication systems. None of the above studies, however, has attempted to characterize wideband CDMA in detail, including the multi-user interference arising from multiple transmitters which is addressed here.

In [5], DOA estimation is assessed using a 6-element linear array. The transmitted signals were carrier-wave tones, sampled at $6ksps$ (kilo samples per second) at baseband. In [6], spatial signature variation, angle spread and beamforming at 1.8 Ghz with 4 or 8 antenna elements is investigated using measurements sampled at $3.072Msps$.

Savahashi and Adachi [7], and Wilson et al. [4] perform experiments on wideband CDMA systems. In [7], BER performance and power delay profiles are measured using a 4-element antenna array, 4-finger Rake combiner, PN chip rate of $15Mcps$, 256-chip orthogonal Gold sequence spreading code with 8-bit A/D at $35Msps$. In [4], diversity combining algorithms are tested by transmitting maximal-length code sequences transmitted at 10 Mcps, and sampling the received IF signal at 40 Msps.

The following experiments are based on a custom-designed antenna array receiver with multiple portable transmitters operating at $1.9GHz$. Features of our experimental system are highlighted in Section II. Resolvable multipath delay statistics and wideband channel dynamics gathered in an outdoor stationary environment are presented in Section III. In Section IV, we perform a statistical study of spatial (multiple antenna) propagation, where we infer the angle spread in our experimental environment. We also study the stability of spatial characteristics generated from repeated experimental trials recorded over time. We apply our measured spatial signatures to an adaptive multi-beam receiver using signal subspace processing in Section V, where we determine potential signal-to-interference plus noise (SINR) improvement from beamforming in a four-user environment.

II. Experimental System Highlights

The key features of our system include: (1) multiple portable transmitters, (2) a basestation receiver with a 4-element antenna array, (3) high chip rate of 7 Mcps, (4) fine sampling resolution of 5 samples per chip, and (5) synchronous coherent I-Q sampling. Photographs appear in Figs. 1 and 2.

The first set of experiments involves a 2-element receiver antenna array (see Fig. 3). Transmitters either operate individually or simultaneously to create scenarios without or with multiuser interference. Transmitters A, B and C, equipped with a single antenna, are separated spatially by 60 degrees and equidistant (50 feet) away from the receiving array. To isolate propagation effects from transients in PN sequence and timing acquisition, local oscillators at all Rx and Tx links are synchronized perfectly by a physical coaxial cable connection to a common reference signal originating from the receiver A/D sampling clock. At least 20 snapshots of 100 bits are acquired synchronously from each antenna at 31 PN chips per bit and 5 samples/PN chip for each scenario.

The second set of experiments uses a 4-element receiver array and four transmitters (see Fig. 4). Each transmitter

N. Tin was with the Dept. of Electrical & Computer Engineering, Queen's University, when this research was conducted. He is now with Bell Mobility, Mississauga, ON, Canada.

S. D. Blostein is with the Dept. of Electrical & Computer Engineering, Queen's University, Kingston, Ontario, K7L 3N6, Canada. † denotes correspondence author. E-mail: sdb@ece.queensu.ca

This research has been supported by the Canadian Institute for Telecommunications Research under the NCE program of the Government of Canada.

is assigned a unique 127-chip PN sequence. Here, 20-40 snapshots of 25 bits each were acquired from each antenna. We remark that the number of simultaneous users is realistic, especially for high rate data transmission. For example, the forthcoming 1xEV-DV 3G standard developing in 3GPP2 supports a maximum of 2 simultaneous packet data users per sector [9].

Both outdoor experiments were conducted in a Queen's University parking lot (see Fig. 5). The receiving antenna array (denoted by "x") and transmitters are in the same location for both experiments, with the addition of TX C for experiment 2. The West and South sides of the test site are surrounded by buildings, East side is partially blocked by two-storey town houses while the North side is open next to a side street. At the time of the second experiment, the parking lot was almost vacated except for a car located midway in the line-of-sight from TX A to the basestation. Using the setup in Fig. 4, a total of 30 snapshots were recorded with four TXs transmitting simultaneously.

III. Multipath and Delay Profiles

A. Multipath Detection and Analysis

Data for multipath delay profile analysis are gathered using a single transmitter and a single-antenna receiver. Delay profiles are generated using a sliding correlator method similar to those described in [1] [10] [11] and [12]. The reliable extraction of (unknown) multipath from the delay profiles involves discriminating signal from background noise due to electronics noise and imperfect sampling. A multipath detection algorithm introduced in [11] is used, which requires an estimate of the background noise variance from experimental data using a sample median. A threshold is set to achieve a constant false alarm rate (CFAR). Since we are interested in resolvable multipaths, the time interval between multipath peaks is assumed to be at least greater than a chip period (5 samples) away from the main peak. A sample delay profile with estimated noise level and the resulting threshold is shown in Fig. 6.

For a single user outdoor environment, transmitter A in Fig. 3 is used, whereas TX A, B and C provide a multi-user environment. The expected noise level of the delay profiles is higher after despreading with MAI present. Based on 20, 100-bit trials for each scenario, the mean multipath amplitudes and delays are similar for both single and multi-user cases. For the multi-user case, the mean delay and delay spread are 2.42 chips and 0.40 chips, respectively.

B. Time Variation of Delay Profiles

To study temporal variation of the delay profiles, consecutive profiles within a 100-bit snapshot are averaged temporally using multiple windows of sizes ranging from 1 to 100 bits. If delay profiles are temporally stable, then averaging consecutive delay profiles within a trial would hardly change the multipath statistics comparing to those with no averaging. This turns out to be true for the 2^{nd} strongest multipath peaks. However results also show that the occurrence of 3^{rd} and 4^{th} peaks are greatly reduced, meaning the more dynamic, lower-amplitude and less frequently occurring peaks are removed by averaging. We conclude that while 3^{rd} and 4^{th} peaks exhibit much more temporally dynamic behavior, their amplitudes are not drastically lower than the 2^{nd} peak amplitudes.

IV. Spatial Channel Characterization

A. Fading Correlation between Antenna elements

The normalized fading correlation provides an estimate of the amount of scattering in the experimental environment [13]. Since the scattering model used in [13] and [14] is based on a single signal source, we calculate the fading correlations using data collected from a single TX in our first outdoor experiment. The receive antenna separation is one half wavelength. We have obtained three separate sets of data gathered for each user A, B or C transmitting individually in Fig. 3.

The fading correlations are calculated using all trials and then on a subset of the trials with no detected multipath. In Table I -60^o, 0^o and 60^o columns denote signals received from TX A, B and C, respectively. Fading correlation values of at least 0.746 corresponds to a low scattering environment with an angle spread of 20^0 or less, according to [13] and [14]. With the multipaths removed, one would expect higher correlation as shown in the right half of Table I. Nevertheless, the values are still significantly below 1.0, especially at a DOA of 0^o, so there is strong evidence of scattering even though a clear line-of-sight exists between Rx and Tx. The correlation values that contain multipaths are unfair comparisons to those in [13] and [14] as their scattering model does not include resolvable multipaths. However, Table I shows that the presence of resolvable multipath reduces the fading correlation values.

B. Spatial Stability of Beampatterns

The array output at time n

$$y_B(n) = \sum_{i=1}^{M} w_i^* x_i(n) = \mathbf{w^H x(n)} \qquad (1)$$

where $*$ represents complex conjugate, H is complex conjugate transpose, $x_i(n)$ is the ith element's received data. The output power is

$$P_B(\mathbf{w}) = \sum_{n=1}^{N_D} |y_B(n)|^2 = \sum_{n=1}^{N_D} |\mathbf{w^H x}(n)|^2 \qquad (2)$$

In the following, we let weight vectors $\mathbf{w}(\theta) = \mathbf{a}(\theta)$, the array response vector corresponding to the uniform linear array (ULA) of our testbed. A beampattern is created by varying θ over an -80^o to $+80^o$ range for $\mathbf{w}(\theta)$ in (2) and calculating $P_B(\mathbf{w}(\theta))$ for a set of angles. A peak in $P_B(\mathbf{w}(\theta))$ represents a DOA estimate of the strongest incoming signal.

The beampatterns for the scenario in Fig. 4 are plotted in Fig. 7, where all trials are superimposed. Spatial signature stabilty is proportional to the alignment of the

beampatterns. Since all four TXs from different directions are transmitting simultaneously, we expect higher peaks in the beampattern at several DOAs as illustrated in Fig. 7.

If the received data is despread with the PN code of user i, i.e., $\mathbf{x}(n)$ in (1) is replaced by despread sequence $\mathbf{y}_{B_i}(n)$, beampatterns are generated for each user corresponding to the strongest path. The beampatterns of despread outputs for users A, B, C and D are shown in Fig. 8. The beampatterns for user B and D have strong peaks around a DOA of 0^o and do not as vary significantly from trial to trial. This suggests that the DOAs of the strongest path for users B and D are rather stable. On the contrary, users A and C show varying beampatterns throughout different snapshots, suggesting that the strongest paths arrive at the antenna array at different angles from users A and C.

This demonstrates that even if transmitters are stationary, other factors in the environment such as cars, human bypassers, building and backyard fences can cause time variations in a beampattern.

V. Beamforming Performance

We apply the experimentally obtained spatial signatures to assess the potential performance of digital beamforming at the basestation in the uplink by adapting a code-filtering approach proposed in [15] to the case where the power of the users are unknown. The method is described in detail in [16]. The received signal model used for beamforming analysis in this section only differs from that of [16] in that the PN codes are complex-valued instead of real, which yield equations that only differ by constant factors.

Beamforming weights are calculated based on two criteria: (1) maximizing SINR (taking into account desired and interfering users' estimated statistics) or (2) maximizing SNR (beamforming to desired user). For the baseline case of no beamforming, the beamforming weight vector is set to unity. The SINR gain from beamforming is calculated for both maximum SINR and maximum SNR beamforming. The SINR gain is calculated separately for each trial for every user and tabulated in Table II for maximum SINR beamforming. The corresponding table for maximum SNR beamforming is not shown due to space considerations. Significant performance differences between maximum SINR and SNR beamformers are evident from our results. The maximum SNR beamformer receives little SINR gain from beamforming, averaging only 0.049 to 0.147 dB for the four users. This suggests that interference cannot be reduced effectively by beamforming towards the desired signal and ignoring the interference. As shown in Table II, maximum SINR beamforming achieves variable gains for different users, ranging from 0.176 dB to 3.335 dB. The maximum gain recorded for an individual trial was 9.96 dB (user C, Trial #2). The SINR gain varies greatly from trial to trial, and beamforming weights need to be re-estimated for each trial (consisting of a 25-bit block) for the SINR to improve.

Finally, we note that gains for users A and C, on average, are much higher than that of users B and D. A plausible explanation is that the spatial signatures of users B and D are similar creating a co-channel interference that cannot be reduced by beamforming. The beampatterns from Fig. 8 seem to support this argument.

VI. Summary and Conclusions

We have evaluated outdoor multipath characteristics for 7 MHz wideband CDMA. While multipath statistics of averaged profiles for the 2^{nd} strongest paths are rather stable in time, this stability does not hold for the weaker paths. We remark that the 3^{rd} strongest path amplitudes were only about 1 dB lower, on average, than the 2^{nd} strongest paths.

The observed fading correlation between antenna elements suggests that the basestation antenna array experiences an angle spread of about 20^o, despite the fact that clear line-of-sight exists and that the receiver-transmitter separations were only 50 feet. The calculated beampatterns indicate that the location of the transmitters with respect to the basestation and its surroundings has a significant effect on the stability of beampatterns.

The data also applied to evaluating SINR enhancement from beamforming using a 2D-RAKE receiver. Using a code-filtering approach, the maximum SINR beamformer was determined without training data or prior information on received signal power or noise density. An average of 0.176 to 3.33 dB SINR gain with four antennas was observed, and varied significantly for different users: user A has an average SINR gain of 2.58 dB over 30 snapshots while users B and D have average gains of only 0.529 and 0.176 dB due to similar spatial characteristics as illustrated by their respective beampatterns.

References

[1] J. Bultitude and G. Bedal, "Propagation Characteristics on Microcellular urban Mobile Radio Channels at 910 mhz," *IEEE JSAC*, pp. 31–39, January 1989.

[2] D.C. Cox, "910 mhz Urban Mobile Radio Propagation: Multipath Characteristics in New York City," *IEEE Trans. Comm.*, pp. 1188–1194, November 1973.

[3] M. Feuerstein and T.S. Rappaport, "Path Loss, Delay Spread, and Outage Models as Functions of Antenna Height for Microcellular System Design," *IEEE Trans. on Vehicular Technology*, pp. 487–498, August 1994.

[4] M. Cotton and P. Wilson, "A Test Bed for the Evaluation of Adaptive Antennas," *Proceeding of 1998 International Symposium on Advanced Radio Technology*, 1998.

[5] R. Muhamed and T.S. Rappaport, "Direction of Arrival Estimation using Antenna Arrays," M.S. thesis, Virginia Polytechnic Institute and State University, 1996.

[6] G.T. Okamoto, *Smart Antenna Systems and Wireless LANs*, Kluwer, 1999.

[7] M. Sawahashi and F. Adachi, "1.92 Mbps data transmission experiments over a coherent W- CDMA mobile radio link," *Proceeding of IEEE VTC '98*, pp. 1300–1304, 1998.

[8] Ward et al., "Characterising the radio propagation channel for smart antenna systems," *Electronics & Communication Engineering Journal*, pp. 191–200, August 1996.

[9] "C50-20020107-002 WG5 Maui meeting summary," *3GPP2 TSG-C contributions*, January 2002.

[10] D.C. Cox, "Delay Doppler Characteristics of Multipath Propagation at 910 mhz in a Suburban Mobile Radio Environment," *IEEE Trans. Ant. Prop.*, pp. 625–635, September 1972.

[11] Sousa et al., "Delay Spread Measurements for the Digital Cellular Channel in Toronto," *IEEE transactions on Vehicular Technology*, pp. 837–847, November 1994.

[12] Jorgensen et al., "Application of Channel Sounding to CDMA PCS Design at 1900 MHz," *IEEE VTC*, pp. 1937–1941, 1997.

[13] J. Salz and J. Winters, "Effect of Fading Correlation on Adaptive Arrays in Digital Mobile Radio," *IEEE Transactions on Vehicular Technology*, pp. 1049–1057, November 1994.
[14] A. Wyglinski, "Mutual Coupling and Scattering Effects on Cellular CDMA Systems Using Smart Antennas," *IEEE VTC-Fall*, pp. 1656–1662, September 2000.
[15] A.F. Naguib, "Performance of wireless CDMA with M-ary orthogonal modulation and cell site antenna arrays," *IEEE JSAC*, pp. 1770–1783, Dec. 1996.
[16] S. Blostein and J. Karimi, "Using Array Signal Processing to Improve Rural Area Coverage in Future Personal Satellite Communications Services," *European Transactions on Telecommunications*, pp. 347–352, July/August 2001.

	All Trials			*Trials without multipaths*		
DOA	-60^O	0^O	60^O	-60^O	0^O	60^O
Mean	0.892	0.746	0.772	0.976	0.837	0.874
Variance	0.019	0.056	0.040	0.002	0.056	0.042

TABLE I
FADING CORRELATION OF TWO ANTENNAS

	SINR gain (dB)			
Trial #	*User A*	*User B*	*User C*	*User D*
1	1.2686	0.2421	0.5478	0.1817
2	0.5657	0.7359	9.9663	0.1242
3	0.8032	0.3068	1.0875	0.1172
4	0.4499	1.0176	7.7437	0.0762
5	2.2636	0.4619	1.8951	0.1316
.	.	.	.	.
.	.	.	.	.
.	.	.	.	.
26	7.2112	0.0638	2.3029	0.1336
27	1.2548	0.6272	1.8578	0.1967
28	1.1770	1.3359	1.6314	0.1032
29	6.6389	0.1764	6.3639	0.1026
30	6.2599	0.4423	1.7677	0.0626
mean	2.5793	0.5288	3.3345	0.1762

TABLE II
SINR GAIN FROM MAXIMUM SINR BEAMFORMING

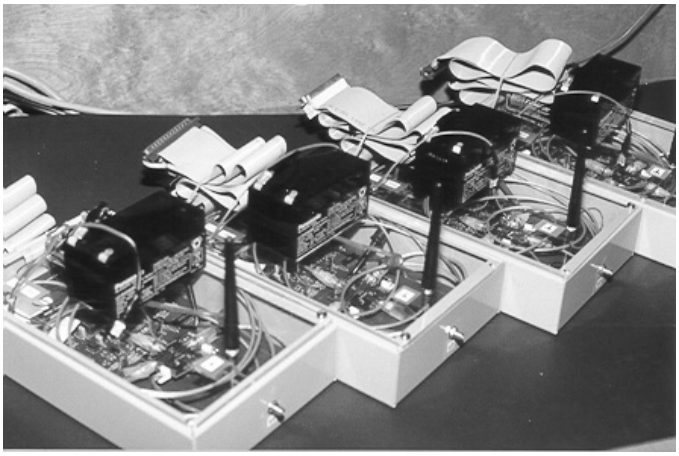

Fig. 1. Photograph of all four portable transmitters

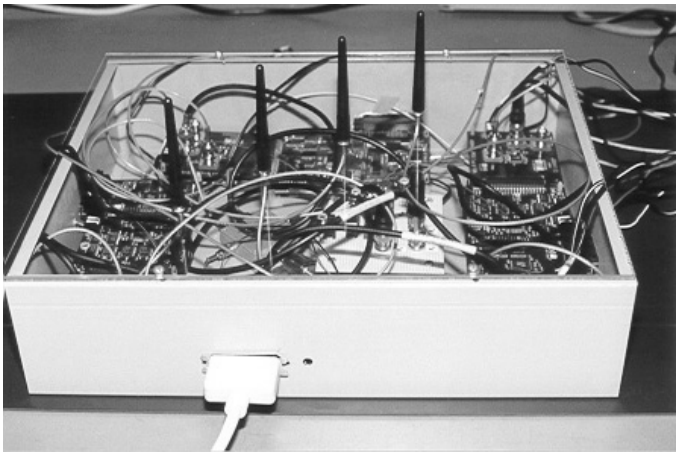

Fig. 2. Photograph of receiving basestation

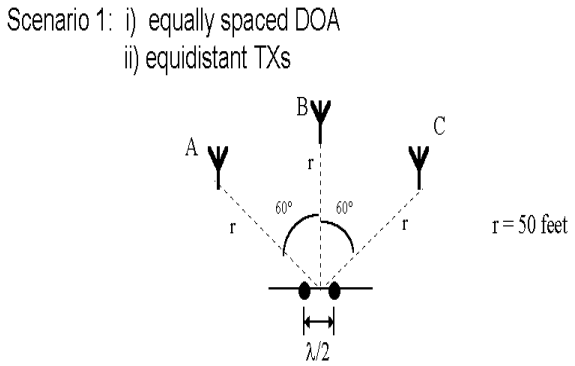

Fig. 3. Outdoor Experiment #1: 3 TXs and 2-element array

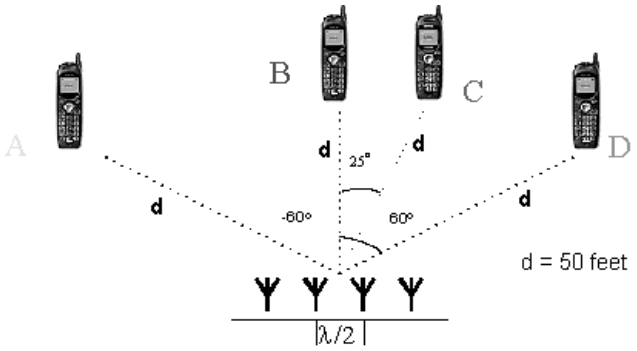

Fig. 4. Outdoor experiment #2: four TXs and 4-element array

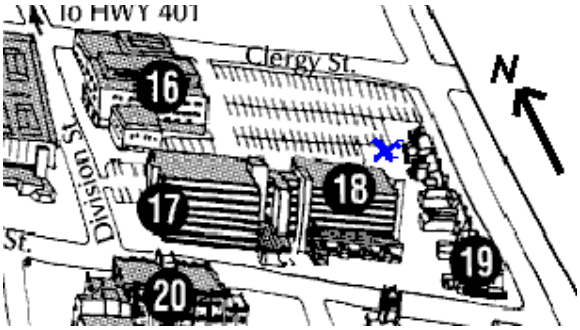

Fig. 5. Outdoor experiment test site

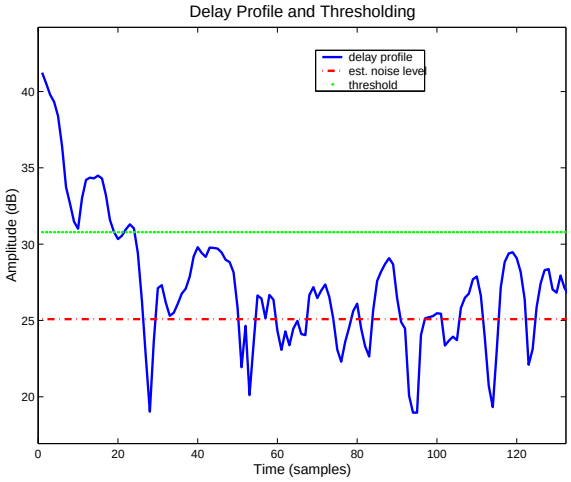

Fig. 6. Delay Profile and Thresholding ($P_{FA} = 10^{-3}$)

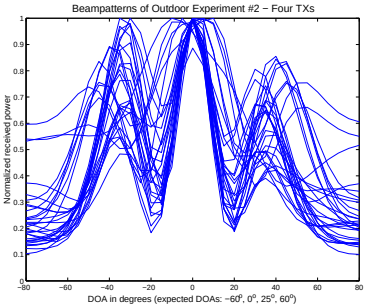

Fig. 7. Beampattern of Outdoor Experiment #2: Scenario 1

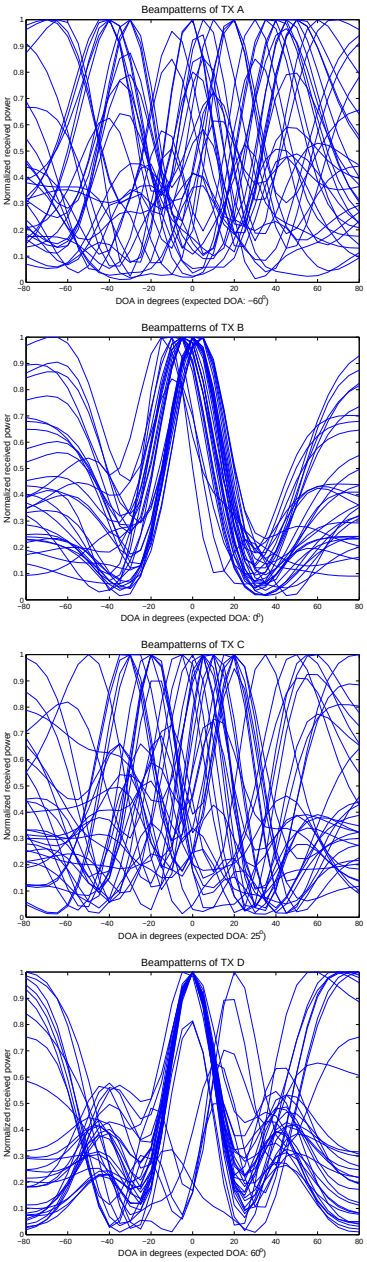

Fig. 8. Top-to-bottom: beampatterns after despreading for users A,B,C, and D.